Environmental Science and Pollution Research (2022) 29:8281–8293
https://doi.org/10.1007/s11356-021-16156-8

RESEARCH ARTICLE

Enhanced degradation of bisphenol S by persulfate activated with sulfide-modified nanoscale zero-valent iron

Jing Cai [1] · Yan Zhang [1]

Received: 13 January 2021 / Accepted: 20 August 2021 / Published online: 5 September 2021

Abstract

Sulfide-modified nanoscale zero-valent iron (S-nZVI) has been considered an efficient material to remove heavy metals and organic contaminants. The experiments of bisphenol S (BPS) degradation by persulfate (PS) activated with S-nZVI (S-nZVI/PS) or nZVI (nZVI/PS) were carried out in this paper. The results show that, compared to the bare nZVI/PS system, the S-nZVI/PS system shows higher activity in BPS degradation, especially at high BPS concentration. The reaction rate constant k_{obs} of BPS removal by the S-nZVI/PS system (0.142 min^{-1}) was much higher than that in nZVI/PS system (0.089 min^{-1}) because more oxidation species were generated in the S-nZVI/PS system. The results of electron paramagnetic resonance (EPR) and radical quenching tests show that both hydroxyl radical (·OH) and sulfate radical ($SO_4^{\cdot-}$) were involved in the degradation of BPS and had a great contribution to BPS removal. Moreover, the effects of S/Fe molar ratio, S-nZVI dosage, initial pH, and initial concentration of PS or BPS on S-nZVI/PS were also studied. The results show that the S/Fe molar ratio has significant influence on the BPS degradation; over 97.7% of the removal efficiency was achieved at 0.035 of S/Fe molar ratio. And the removal efficiency of BPS degradation increased with the increase of the dosage of S-nZVI, PS concentration. Furthermore, BPS could be efficiently removed in solutions with a wide range of initial pH (3.13–9.35). The observed results show that it is promising in the removal of micro-pollutants from water by persulfate activated with S-nZVI.

Keywords Sulfide-modified nanoscale zero-valent iron (S-nZVI) · Persulfate · Bisphenol S degradation · Sulfate radical ($SO_4^{\cdot-}$) · Hydroxyl radical (·OH)

Introduction

Bisphenol S (BPS), as a substitute for bisphenol A (BPA), has been already commonly used in the synthesis of thermal receipts, plenty of plastics, epoxy resins, infant feeding bottles, etc. (Ahsan et al. 2018, Champmartin et al. 2020). Recent studies have reported that BPS also appears to have some endocrine-disrupting effects on human, similarly to BPA (Azevedo et al. 2020, Champmartin et al. 2020). Furthermore, studies have shown that BPS is resistant to degradation in the environment, being persistent and thus prone to contaminate humans and wildlife (Freitas et al. 2020). Consequently, it is extremely necessary to adopt an effective and fast measure for elimination of BPS from water.

Presently, some strategies like adsorption (Yang et al. 2020) and biodegradation (Danzl et al. 2009) have been tested to remove BPS from water. However, these methods usually suffered from the disadvantages of incomplete degradation, such as low efficiency, long reaction time, and high cost.

Up to now, advanced oxidation processes (AOPs) based on persulfates have received extensive attention for the degradation of many organic contaminants, such as sulfadiazine (Roy et al. 2020), sulfamethazine (Dong et al. 2020), nonylphenol (Hussain et al. 2017), and atrazine (Jiang et al. 2020). Various methods such as ultraviolet irradiation (Lu et al. 2019) and heating (Wang et al. 2017) have been developed in activating persulfates to generate sulfate radical ($SO_4^{\cdot-}$) with a high standard oxidation–reduction potential (E (SO.− 4/SO2− 4) = 2.43 V) for the oxidation of organic pollutants (Eqs. (1) and (2)). Mercado et al. found that the fungicide flusilazole chemically reacts with sulfate radical anion with rate constant of 4.6×10^8 s^{-1} M^{-1} (Mercado et al. 2018a). However, these techniques

Responsible Editor: Ricardo A. Torres-Palma

✉ Yan Zhang
zhangyan@zju.edu.cn

[1] Department of Civil Engineering, Zhejiang University, 866 Yuhangtang Road, Hangzhou 310058, China

require high-energy inputs and hard reaction conditions, which are not cost-effective for water treatment (Wang et al. 2019).

$$S_2O_8^{2-} \rightarrow^{\text{activator}(e^-)} SO_4^{\cdot-} + SO_4^{2-} \quad (1)$$

$$S_2O_8^{2-} \rightarrow^{\text{energy input}(e^-)} SO_4^{\cdot-} + SO_4^{2-} \quad (2)$$

By comparison, transition metal irons, such as Fe^{2+} (Ning et al. 2020), Ag^{+} (Zhang et al. 2020), Co^{2+} (Gayathri et al. 2010), and Cu^{2+} (Fu et al. 2020), are recognized as efficient reagents for persulfate activation. Among these transition metal irons, Fe^{2+} is widely used for activation of persulfate due to its nontoxicity and low cost (Ning et al. 2020). Although persulfate activated with Fe^{2+} has been reported for the degradation of numerous organic contaminants, the scavenging of reactive oxygen radicals (ROSs) by excess concentration of Fe^{2+} could highly reduce the oxide capacity of system (Eq. (3)) (Dong et al. 2020). Moreover, this system has issues of the generation of iron hydroxide precipitates. Therefore, heterogeneous systems involving solid particles of zero-valent iron (Fe^0) or iron oxides have been used as an alternative (Roy et al. 2020). Particularly, nanoscale zero-valent iron (nZVI) has been attracting considerable attention due to its small particle size, excellent reactivity, high specific surface area, and non-toxicity (Wu et al. 2020). Furthermore, nZVI shows better performance of activating persulfate than Fe^{2+} because Fe^{2+} can be slowly released by dissolved oxygen and persulfate (Eqs. (4) and (5)) in the nZVI/PS system (Kim et al. 2020), which avoids $SO_4^{\cdot-}$ being scavenged by excess Fe^{2+}. Then, the released Fe^{2+} could activate persulfate to generate $SO_4^{\cdot-}$ (Eq. (6)), which results in higher removal efficiency of the pollutants. However, nZVI can be easily aggregated and oxidized because of their small size and magnetic interaction between particles, which resulted in a decrease in reactivity (Yan et al. 2015).

$$SO_4^{\cdot-} + Fe^{2+} \rightarrow SO_4^{2-} + Fe^{3+} \quad (3)$$

$$2Fe^0 + O_2 + 2H_2O \rightarrow 2Fe^{2+} + 4OH^- \quad (4)$$

$$Fe^0 + S_2O_8^{2-} \rightarrow Fe^{2+} + 2SO_4^{2-} \quad (5)$$

$$Fe^{2+} + S_2O_8^{2-} \rightarrow Fe^{3+} + SO_4^{\cdot-} + SO_4^{2-} \quad (6)$$

Recently, sulfide-modified nanoscale zero-valent iron (S-nZVI) has received more attention due to its many advantages over nZVI; S-nZVI composites exhibit some steric stability and lower magnetic properties ascribed to the generation of iron sulfides on its surface (Han and Yan 2016, Song et al. 2017). In addition, the sulfidation of nZVI could improve the selectivity for the reduction of contaminants and extend the reactive lifetime by slowing the reaction with water (Cao et al. 2017). Most importantly, the iron sulfides which replaced the iron oxides on the surface of S-nZVI could enhance electron transfer and depassivation capacities of the iron surface (Kim et al. 2011, Li et al. 2019, Rayaroth et al. 2017). Kim et al. and Su et al. found that the S-nZVI composites with a proper Fe/S ratio exhibited a larger adsorption capacity than pristine nZVI (Kim et al. 2014, Su et al. 2015). Thus, S-nZVI was widely used to reduce heavy metals and organic contaminants (Dong et al. 2018, Fu et al. 2015, Jia et al. 2019).

However, little studies have focused on S-nZVI-activated persulfate (S-nZVI/PS) to degrade organic compounds. Dong et al. (2019) found that S-nZVI composites showed better performance for activating PS than nZVI, due to the higher iron dissolution rates and iron sulfides (e.g., FeS and FeS_X) generated on its surface, which accelerated the transfer rate of electrons for activating PS (Dong et al. 2019). Rayaroth et al. (2017) reported that 100% of benzoic acid (BA) could be removed by persulfate activated with nFe/FeS at alkaline pH, while in the case of persulfate activated with Fe^0, the degradation rate decreased to 8% (Rayaroth et al. 2017). Besides, Liu et al. synthesized a Fe-based activator (Fe@C) and evaluated the activation performance of the Fe@C/peromonosulfate (PMS) system on the degradation of BPS. The results showed that about 80% of BPS could be removed by 0.5 g/L catalyst activated PMS in 30 min (Liu et al. 2019). The S-nZVI/PS system shows high efficiency, and low dosage is required for removing contaminants from the aqueous system. Thus, it is proposed that the S-nZVI/PS system may enhance the BPS removal efficiency; however, to our knowledge, no corresponding literature can be found so far.

In this study, the experiments of BPS degradation by PS activated with nZVI or S-nZVI were systematically carried out. The main active species from BPS degradation by the S-nZVI/PS system have been elucidated based on the electron paramagnetic resonance spectra (EPR) and classical quenching tests; the mechanism of BPS degradation by PS activated with S-nZVI was discussed. Moreover, the effects of reaction parameters on BPS degradation have been systematically investigated, such as S/Fe molar ratio, S-nZVI dosage, initial pH, PS, and BPS concentration. The goal of this study is to determine a promising effective and economical method for the BPS degradation from water.

Materials and methods

Materials

Ferrous sulfate heptahydrate ($FeSO_4 \cdot 7H_2O$), sodium borohydride ($NaBH_4$), sodium dithionite ($Na_2S_2O_4$), sodium hydroxide (NaOH), hydroxylamine hydrochloride ($HONH_2HCl$), sodium bicarbonate ($NaHCO_3$), ammonium acetate (CH_3COONH_4), sulfuric acid (H_2SO_4), hydrochloric acid (HCl), and ethanol (EtOH) were obtained from Sinopharm Group Chemical Reagent (Shanghai, China). Bisphenol S,

sodium persulfate ($Na_2S_2O_8$), potassium iodide (KI), phosphate acid, and tertiary butanol (TBA) were purchased from Aladd in Bio-Chem Technology Co., Ltd. 1,10-phenanthroline was supplied by Macklin Biochemical Co., Ltd (Shanghai, China). Polyvinylpyrrolidone (PVP, K-30) was purchased from Nantong Feiyu Biotechnology Co., Ltd. (Nantong, China). Methanol was purchased from Merck (Germany).

Synthesis of nZVI and S-nZVI

The nZVI particles were synthesized by a liquid-phase reduction method (Cai and Zhang 2020). More details are listed in the Supporting Information (SI).

Characterization of nZVI and S-nZVI

The surface areas of nZVI and S-nZVI particles were calculated by the Brunauer-Emmett-Teller (BET). The morphology of the samples was characterized by transmission electron microscopy (TEM, HITACHI, HT7700, Japan) and scanning electron microscopy (SEM, FEI, FEG650, China). The X-ray diffraction pattern of the samples was recorded using an X-ray diffractometer (XRD, Shimadzu, XRD-7000, Japan) operated with Cu Kα radiation, a 40-kV voltage, and a 40-mA current. The patterns of the samples were recorded from 5 to 80° (in 2θ) with a 0.02° step width and a scanning rate of 2.4° min^{-1}. The surface elemental compositions of the materials were determined by X-ray photoelectron spectroscopy (XPS, VG ESCALAB Mark II, UK).

Batch experiments

The batch experiments of degradation of BPS were conducted in a 100-mL three-necked flask at water bath (25 °C) exposed to the atmosphere. The reaction was initiated by adding an aliquot of the BPS solution and persulfate stock solution to give initial concentration of 20 μM BPS and 1 mM persulfate. Then, a predetermined amount of materials (nZVI or S-nZVI) were added into the reactor. The adsorption–desorption equilibrium of the BPS on the nanomaterials was guaranteed before the catalytic experiments. The pH of the solution was not further adjusted except the experiments of the effect of pH on BPS degradation. And no buffer solutions were added during the experiment in this study. Water samples were taken at different times (i.e., 1, 3, 5, 10, 15, 20, 30 min) and filtered through a 0.22-μm membrane filter; 50 μL methyl alcohol and 20 μL ascorbic acid were immediately added to the solutions to quench the oxidation process. Finally, samples were collected for subsequent analyses.

In order to figure out the effects of pH, the pH of the solutions was adopted by 0.1 M H_2SO_4 and 0.1 M NaOH.

Unless otherwise specified, the experiments were conducted with nZVI or S-nZVI(S/Fe = 0.035), pH, temperature, initial BPS, and persulfate concentrations of 30 mg/L, 5.6 ± 0.2, 25 °C, 20 μM, and 1 mM, respectively. All experiments were conducted in triplicate. The data reported here were the average of three replicated experiments, and error bars represent the standard deviation of the averages.

Reactive species scavenging tests were performed to evaluate the contribution of each reactive species to BPS oxidation. Tertbutyl alcohol (TBA) was added before the reactions were initiated to scavenge ·OH, while methanol (MeOH) was added before the reactions were initiated to scavenge ·OH and $SO_4^{\cdot-}$.

To test the reusability of S-nZVI, the particles were collected by a magnet and washed three times with ultrapure water after each run. Then, the washed S-nZVI was dried in a vacuum oven before the next run.

Analytical procedures

The concentration of BPS was determined by high-performance liquid chromatography (HPLC) analysis equipped with a C18 column (4.6 × 250 mm, 5 μm) and a UV detector. In general, the mobile phase consisted of 0.1% phosphate acid and acetonitrile with a ratio of 70:30 (vol./vol.) at a flow rate of 1 mL/min. The injection volume was 20 μL. The detector temperature and the wavelength were set at 35 °C and 256 nm, respectively. The oxidation–reduction potential (ORP) and pH of the solution were measured by a Hach HQ40d MI-parameter meter (HACH, USA). The formation of $SO_4^{\cdot-}$ and ·OH during the process was detected by electron paramagnetic resonance spectra (EPR, Bruker A300 EPR Spectrometer, Germany), and 5,5-dimethyl-1-pyrroline-N-oxide (DMPO) was employed as the radical spin trapping reagent.

The persulfate concentration was determined using a spectroscopic method (Liang et al. 2008). The 1,10-phenanthroline method was used to determine the dissolved iron concentration. The concentrations of PS and dissolved iron were determined by the absorption peaks at 352 nm and 510 nm, respectively, using a UV-vis spectrophotometer (Hach, DR6000, USA).

3.Results and discussion

3.1.Physicochemical properties of nZVI and S-nZVI

The structure and morphology of nZVI and S-nZVI were characterized by SEM and TEM; the results are shown in Fig. 1. From the SEM and TEM images of nZVI (Fig. 1 a and c), it is clear that nZVI particles aggregated in chain-like structures due to the magnetic forces and electrostatic

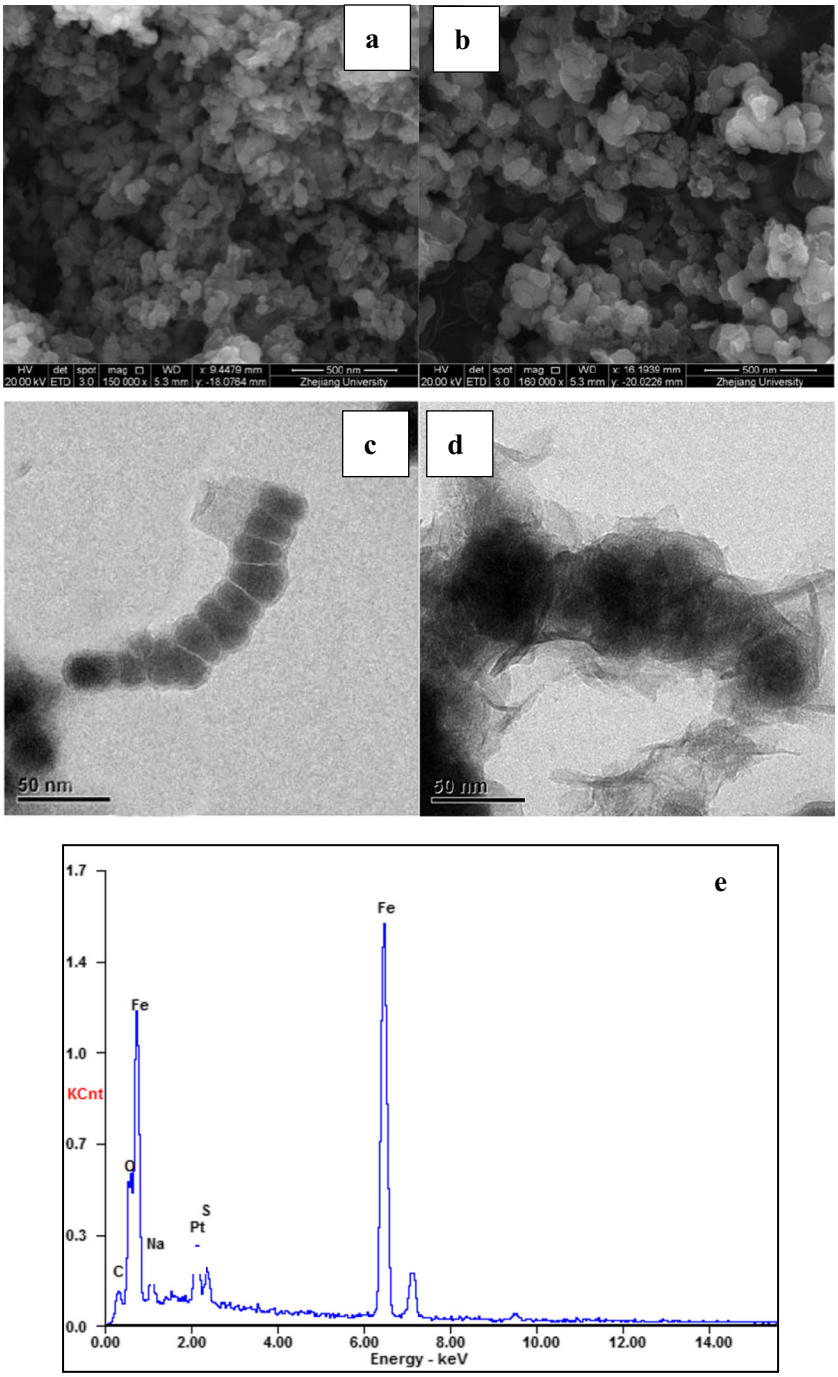

Fig. 1 SEM and TEM images of nZVI (**a**, **c**) and S-nZVI (**b**, **d**); EDS image of S-nZVI (**e**)

interactions (Mercado et al. 2018b). Moreover, the TEM image of nZVI given in Fig. 1c shows that each spherical particle contained an iron core surrounded by a thin oxide shell less than 4 nm in thickness, which resulted from oxidation during the synthesis process (Mercado and Weiss 2018). Figure S1 shows nZVI with primary particle diameters between 20 and 60 nm.

The SEM image of S-nZVI (Fig. 1b) shows that S-nZVI aggregated in string-like clusters rather than the typical chain-like structures of nZVI (Han and Yan 2016), which might be explained that the iron sulfide coating decreases the magnetic attractions between the particles (Su et al. 2015). And the TEM image of S-nZVI (Fig. 1d) exhibits a slightly different "flake-like-shell" morphology. Figure S2 shows that S-nZVI are almost spherical (diameter ~ 100 nm) though flaky. N_2 adsorption isotherms (Fig. S3) of nZVI and S-nZVI show that the BET surface areas of nZVI and S-nZVI are 5.40 and 15.53 m^2/g, respectively. This finding was also reported by Su et al. (2015), who reported that S-nZVI has much higher surface to volume ratio due to the abundant flake-like structure,

compared with nZVI. The higher BET surface area of S-nZVI may have contributed to higher adsorption capacity and providing more active sites for activating PS. Besides, from the EDS data (Fig. 1e), it is evident that S-nZVI composites contain S in addition to Fe and O, indicating that iron sulfides were successfully formed on the surface of S-nZVI.

The XRD patterns of both the iron nanoparticles are shown in Fig. 2. This pattern shows that nZVI has main diffraction peaks at 2θ = 44.6 and 64.8°, responding to the (110) and (200) planes of α-Fe, respectively (Fig. 2a). The results confirm the existence of Fe^0 in the nZVI particles and suggest the high degree of crystallinity of nZVI. As shown in Fig. 2b, the Fe^0 peak of S-nZVI is less pronounced than nZVI and the intensity is weakened due to the coverage of amorphous iron sulfides, indicating that the sulfidation process decreases the crystallinity of Fe^0 in the particles, which is consistent with some previous studies (Du et al. 2016, Su et al. 2016, Su et al. 2015). Meanwhile, the diffraction peaks corresponding to iron sulfide and iron disulfide can not be directly observed, which might be attributed to their low concentrations or low degree of crystallinity (Rayaroth et al. 2017). Some new diffraction peaks ascribed to Fe_2O_3 (maghemite iron oxide) and FeO(OH) can be found in the XRD patterns of S-nZVI after a 30-min reaction with BPS (Fig. 2b). The results indicate that the corrosion products were iron oxides and iron hydroxides in the system achieving BPS removal by S-nZVI/PS. Meanwhile, the weak diffraction peak of Fe^0 shows that Fe^0 was consumed during the reaction.

BPS degradation by nZVI or S-nZVI

The performance of BPS degradation by PS, nZVI, S-nZVI, nZVI/PS, and S-nZVI/PS system is shown in Fig. 3. As can be seen, the removal of BPS was negligible in the treatment of PS alone, indicating that the oxidation ability of PS was limited under the condition without any activator (Hussain et al. 2017). The concentration of BPS could be reduced by nZVI alone to some degree within 5 min, and S-nZVI alone showed a slightly higher BPS removal rate than nZVI alone.

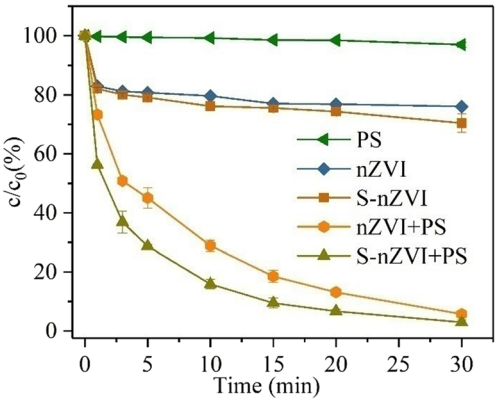

Fig. 3 The degradation of BPS in different systems. Conditions: $[PS]_0$ = 1.0 mM, $[BPS]_0$ = 20 μM, [nZVI] = [S-nZVI] = 30 mg/L, pH = 5.6 ± 0.2, T = 25 °C

However, whether in the nZVI or S-nZVI system, much better performance in the degradation of BPS was observed by the addition of PS. This may be explained as follows. On the one hand, it was extremely necessary for PS to have an activator to accelerate the oxidation process. Fe^{2+} generated by nZVI and S-nZVI had the ability to induce PS to produce $SO_4^{\cdot-}$ and ·OH (Dong et al. 2019, Kim et al. 2018). On the other hand, the significant increase pertaining to BPS removal rate revealed that the radicals produced in the nZVI/PS and S-nZVI/PS systems played an important role in the degradation of BPS.

In addition, S-nZVI was found to be more efficient than nZVI in activating PS to degrade BPS, especially at high BPS concentration (Fig. 4). It might be attributed to the aggregation of nZVI particles and the passivation layer formed on the surface of nZVI (Xu et al. 2020), and thus decreased the ability of BPS removal. Contrarily, S-nZVI could effectively avoid the aggregation of iron particles and reduce the

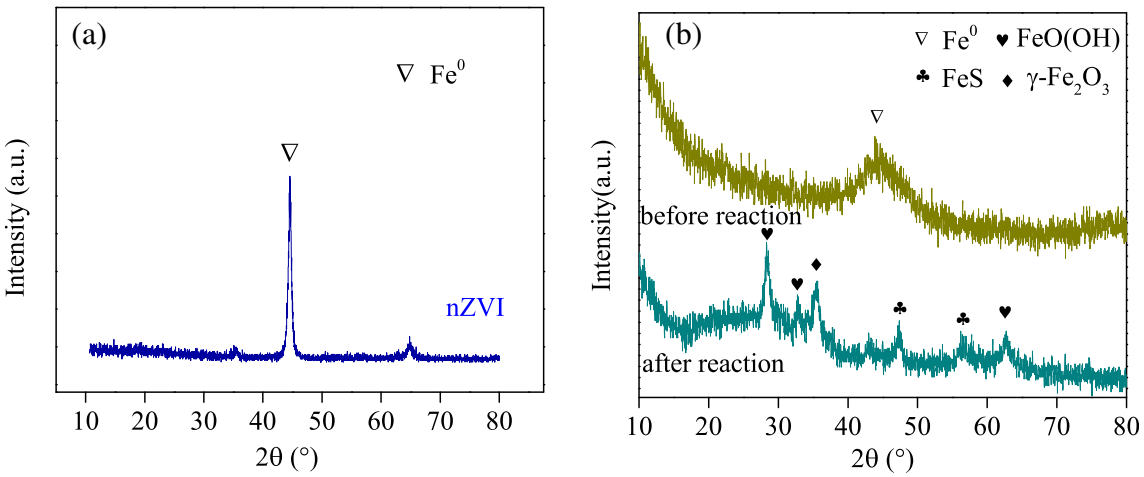

Fig. 2 XRD pattern of nZVI (**a**); S-nZVI before and after reaction (**b**)

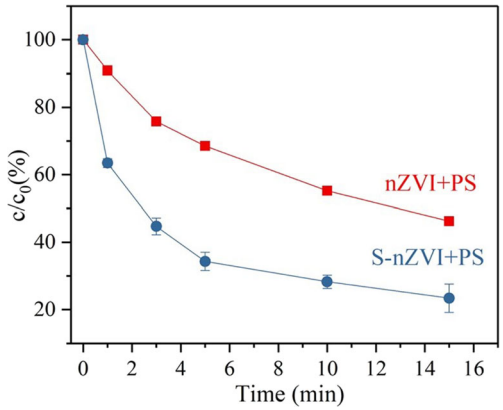

Fig. 4 The degradation of BPS in nZVI/PS and S-nZVI/PS systems. Conditions: $[PS]_0$ = 1.0 mM, $[BPS]_0$ = 40 μM, [nZVI] = [S-nZVI] = 30 mg/L, pH = 5.6 ± 0.2, T = 25 °C

generation of iron oxide on the surface of particles because of the addition of an iron sulfide layer, and the transfer of electrons could be enhanced at an appropriate molar ratio of S/Fe. As a result, it could be inferred that it was highly possible that the introduction of iron sulfides reinforced the oxidation capacity of the S-nZVI/PS system for BPS removal. The observed change could be further explained based on the iron dissolution and persulfate decomposition, given in the "nZVI and S-nZVI corrosion and persulfate decomposition" section.

Effects of S/Fe molar ratio

The effects of S/Fe molar ratio on BPS degradation by S-nZVI/PS were investigated, and the results are shown in Fig. 5. On the whole, a certain extent sulfidation of nZVI could increase the removal efficiency of BPS compared with the bare nZVI.

From Table 1, the reaction rate constant k_{obs} was increased from 0.089 to 0.142 min^{-1}, when S/Fe molar ratio increased from 0 to 0.035. But the removal efficiency obviously decreased when further increasing the S/Fe molar ratio to 0.14 and 0.28, and the reaction rate constant decreased to 0.087 min^{-1} and 0.048 min^{-1}, respectively. The maximum removal efficiency of 97.7% and the maximum k_{obs} of 0.142 min^{-1} of BPS removal by S-nZVI/PS were achieved at a S/Fe molar ratio of 0.035. The different S/Fe molar ratios indicate different iron sulfide compounds (e.g., FeS, FeS_X) may be formed on the surface of nZVI. The enhanced reactivity of nZVI by sulfidation should be ascribed to the formation of FeS and FeS_X; the electron transferring from the Fe^0 core to the surface is accelerated by the existence of doped FeS (Rajajayavel and Ghoshal 2015). Fe^{2+} is released by FeS on the surface of S-nZVI, and then PS is activated to generate $SO_4^{\cdot-}$. Because of the higher electronegativity of FeS (5.02 eV) than that of nZVI (4.04 eV), electrons generated by nZVI corrosion could be spontaneously transferred to the FeS semiconductor, which could reduce Fe^{3+} to Fe^{2+} (Sun et al. 2020). However, with the increasing of S/Fe molar ratio, in the synthesis process of S-nZVI, the excessive amount of sulfur might generate iron polysulfide compounds (FeS_X), which have a much lower reactivity than FeS (Han and Yan 2016). Meanwhile, the excessive $S_2O_4^{2-}$ might be decomposed into sulfite (SO_3^{2-}) and sulfate (SO_4^{2-}) (Eqs. (15)–(17)), which would deposit onto the surface of Fe^0 and then influence the electron transfer between Fe^0 and PS (Dong et al. 2018), and therefore reduce the removal efficiency of BPS. Consequently, the degradation rate of BPS by S-nZVI/PS was accelerated at a low S/Fe molar ratio and decreased with further increase of the S/Fe molar ratio.

$$2S_2O_4^{2-} + H_2O \rightarrow 2SO_3^{2-} + S_2O_3^{2-} + 2H^+ \quad (7)$$

$$2SO_3^{2-} + H_2O \rightarrow 2SO_4^{2-} + 4e^- + 4H^+ \quad (8)$$

$$S_2O_3^{2-} + 5H_2O \rightarrow 2SO_4^{2-} + 8e^- + 10H^+ \quad (9)$$

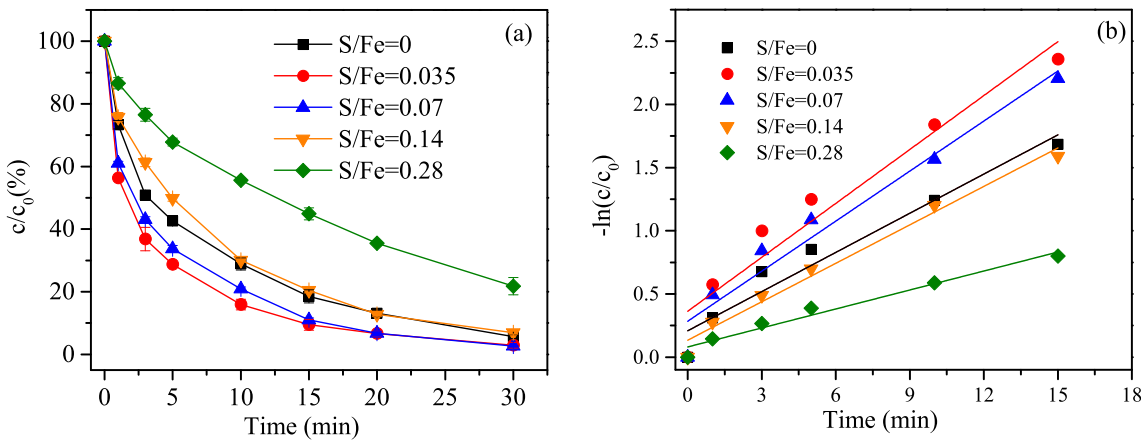

Fig. 5 Effects of S/Fe molar ratio on the degradation of BPS. Conditions: $[PS]_0$ = 1.0 mM, $[BPS]_0$ = 20 μM, [nZVI] = [S-nZVI] = 30 mg/L, pH = 5.6 ± 0.2, *T* = 25 °C

Table 1 First-order kinetic parameters of BPS removal by S-nZVI/PS (effect of PS concentration and S/Fe molar ratio)

PS concentration (1.0 mM)	S/Fe molar ratio (0.035)		S/Fe molar ratio	PS concentration (1.0 mM)	
	k_{obs} (min^{-1})	R^2		k_{obs} (min^{-1})	R^2
0.5	0.075	0.85	0	0.089	0.98
1.0	0.142	0.95	0.035	0.142	0.95
2.0	0.160	0.99	0.07	0.132	0.98
5.0	0.418	0.99	0.14	0.087	0.98
10.0	1.336	0.98	0.28	0.048	0.99

nZVI and S-nZVI corrosion and persulfate decomposition

To reveal the activation mechanism of PS in nZVI/PS and S-nZVI/PS systems, the iron dissolution during the degradation of BPS was investigated. The results are presented in Fig. 6. The concentration of Fe^{2+} in nZVI/PS or S-nZVI/PS system gradually increased with the increasing of reaction time. The Fe^{2+} released by nZVI/PS or S-nZVI/PS was easily transformed into Fe^{3+}. Meanwhile, the concentration of total iron in the S-nZVI/PS system increased faster and slightly higher than that in the nZVI/PS system. This phenomenon could be ascribed to the formation of a passive film on the surface of nZVI, resulting in a decrease of the iron dissolution rate, while the S-nZVI/PS system indeed had the advantage of releasing Fe^{2+} by accelerating the transfer rate of electrons for activating PS in the presence of iron sulfides. S-nZVI particles are more susceptible to electron donation due to the presence of sulfides, which are more hydrophobic than iron oxides (Rayaroth et al. 2017). Furthermore, Fe^{2+} could activate PS to generate $SO_4^{\cdot-}$ further to remove BPS; the consumption of Fe^{2+} during PS activation accelerates the transformation of Fe^0 and the formation of Fe^{3+}, and part of Fe^{3+} could be reduced to Fe^{2+}. Therefore, higher iron dissolution rates of S-nZVI and iron sulfides (e.g., FeS and FeS_X) generated on its surface might provide more electrons for activating PS to generate more free radicals and finally elevate the degradation efficiency of BPS.

The persulfate decomposition during the BPS degradation is presented in Fig. 7. It is obvious that only a small portion of persulfate was consumed during the BPS degradation by nZVI/PS. This may be due to the recombination of sulfate radicals and the formation of iron oxides on the surface of nZVI, and then inhibiting the reaction with PS. However, it shows a remarkable decomposition of PS while removing BPS by S-nZVI/PS. Compared to nZVI, S-nZVI could be easily affected by electron donor due to the iron sulfides. Iron sulfides are more hydrophobic than iron oxides and can easily react with persulfates by electron transfer to generate radicals (Rayaroth et al. 2017).

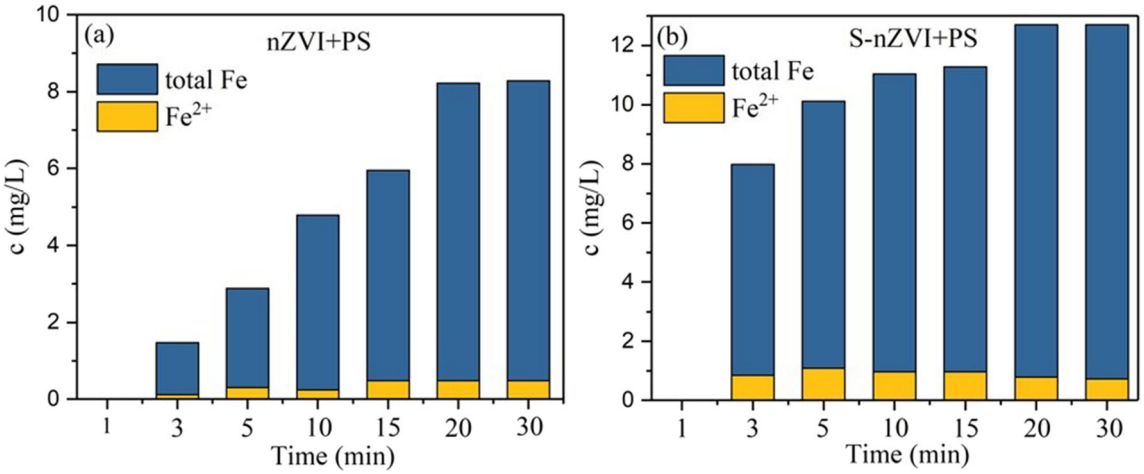

Fig. 6 The iron dissolution during the degradation of BPS in **a** nZVI/PS and **b** S-nZVI/PS systems. Conditions: $[PS]_0$ = 1.0 mM, $[BPS]_0$ = 20 μM, [nZVI] = [S-nZVI] = 30 mg/L, pH = 5.6 ± 0.2, T = 25 °C

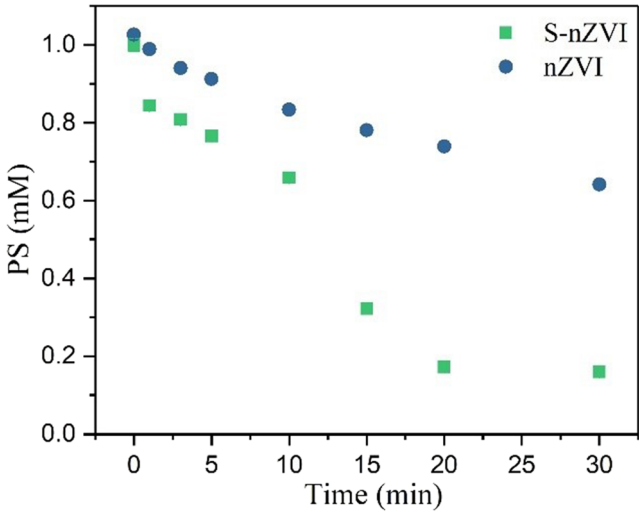

Fig. 7 The persulfate decomposition during the degradation of BPS. Conditions: $[PS]_0$ = 1.0 mM, $[BPS]_0$ = 20 μM, [nZVI] = [S-nZVI] = 30 mg/L, pH = 5.6 ± 0.2, T = 25 °C

Variation in the ORP and pH during the reaction

The changes of pH and ORP values of solution during the degradation of BPS are given in Fig. 8. The ORP value of the solution quickly increased as the reaction progress both in nZVI/PS and S-nZVI/PS systems. However, the ORP value increased faster in the S-nZVI/PS system than that in the nZVI/PS system. And the higher ORP value demonstrated that more oxidation species were generated in the S-nZVI/PS system, which could contribute to the higher removal efficiency of BPS.

The pH value decreased to approximately 3.2 in 5 min and remained at that value throughout the BPS degradation process. However, higher iron dissolution, PS consumption, and BPS removal efficiency could be found in the S-nZVI/PS system compared to that in the nZVI/PS system at similar pH, because partial sulfidation of nZVI could improve the limitation of passivation and accelerate electron transfer.

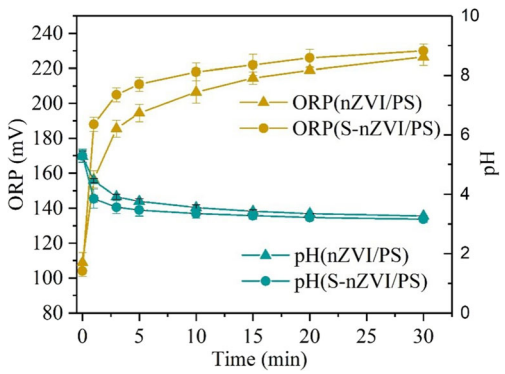

Fig. 8 Variation in ORP and pH during the degradation of BPS using nZVI and S-nZVI. Conditions: $[PS]_0$ = 1.0 mM, $[BPS]_0$ = 20 μM, [nZVI] = [S-nZVI] = 30 mg/L, pH = 5.6 ± 0.2, T = 25 °C

XPS analysis of S-nZVI

To further explain the excellent removal efficiency of BPS by S-nZVI/PS, the composition of S-nZVI before and after the reaction was compared by performing XPS characterization and the results are shown in Fig. 9. For the Fe 2p spectra of S-nZVI (shown in Fig. 9a) before the reaction, the binding energies at 710.4 eV and 711.8 eV were attributed to $Fe2p_{3/2}$ of Fe (II) and Fe (III), respectively; and the peaks at 723.8 eV and 725.6 eV were assigned to $Fe2p_{1/2}$ of Fe (II) and Fe (III), respectively. After the reaction (shown in Fig. 9c), the increase in the Fe (III) peak intensity shows that part of Fe^{2+} was oxidized to Fe^{3+} after the reaction. The S 2p spectra of S-nZVI (shown in Fig. 9b) before the reaction demonstrate that a mixture of sulfur phases was present on the particles, including SO2- 4, SO2- 3, and polysulfide (S2- n). After the reaction (shown in Fig. 9d), the S 2p spectrum consists of two peaks corresponding to SO_3^{2-} and SO_4^{2-} groups, indicating the oxidation of the iron sulfides.

Identification of reactive oxygen species (ROS) and their formation

In order to confirm the dominant oxidizing species in the S-nZVI/PS system, radical-scavenging experiments were performed by using scavengers such as methanol (MeOH) and tertiary butanol (TBA). The results are presented in Fig. 10. The second-order rate constants for MeOH reaction with ·OH and $SO_4^{\cdot-}$ are 0.8–1.0 × 10^7 and 0.9–1.3 × 10^9 L/mol/s, respectively (Hussain et al. 2017). The rate constants for TBA reaction with ·OH and $SO_4^{\cdot-}$ are 3.8–7.6 × 10^8 and 4.9–9.1 × 10^5 L/mol/s, respectively. Thus, MeOH is an effective scavenger for $SO_4^{\cdot-}$ and ·OH, and TBA is a strong quenching agent for ·OH. It could be found from Fig. 8 that the BPS removal efficiency decreased from 97.7% to 26.0% and 67.8% with the addition of MeOH and TBA, respectively. The relative contributions of $SO_4^{\cdot-}$ and ·OH were 42.78% and 30.60%, respectively. The result suggests that both $SO_4^{\cdot-}$ and ·OH were involved in the degradation of BPS by PS activated with S-nZVI.

In addition, the radical species associated with the oxidation of BPS were further detected by the EPR technique. As illustrated in Fig. 11, EPR signals of both DMPO-·OH and DMPO-$SO_4^{\cdot-}$ could be observed. The intensity of DMPO-·OH adduct generated in the S-nZVI/PS system was relatively higher than DMPO-$SO_4^{\cdot-}$; it might result from the strong acidic solution during the reaction process so that partial $SO_4^{\cdot-}$ was transformed to ·OH. And previous report pointed that $SO_4^{\cdot-}$ can be retained for a very short time when persulfate was activated by transition metal ion (Wu et al. 2014). These results indicate that the S-nZVI/PS system could activate PS to a certain extent to form $SO_4^{\cdot-}$ and ·OH, which was similar to a previous report on atrazine removal by ZVI/BC-activated PS (Jiang et al. 2020).

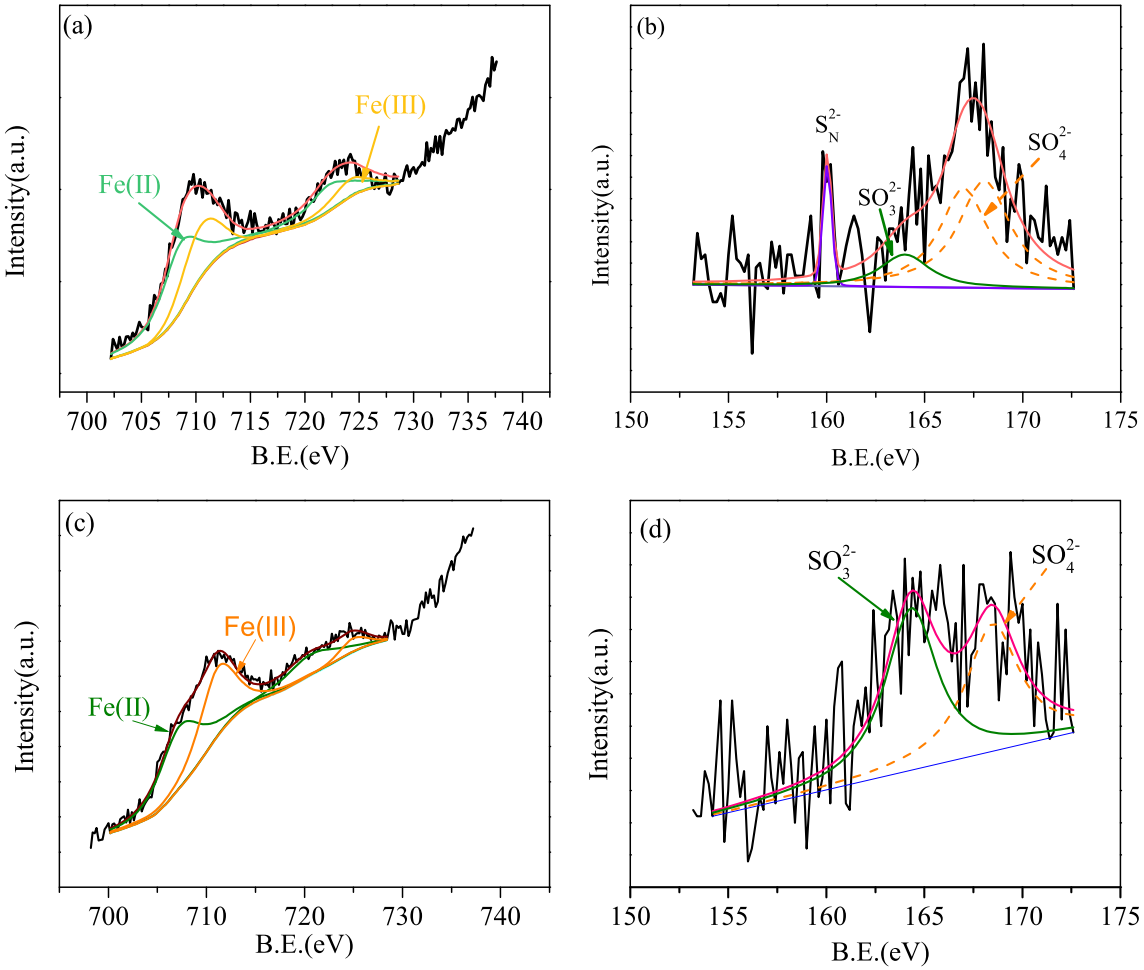

Fig. 9 Fe 2p and S 2p XPS spectra of S-nZVI (**a**, **b**) before and after 30-min reaction (**c**, **d**)

Mechanism of persulfate activated with S-nZVI

It has been demonstrated that PS can be quickly activated by S-nZVI to generate free radicals, and thus, the S-nZVI/PS system exhibits a higher degradation efficiency of BPS than the nZVI/PS system, indicating that the property of nZVI for PS activation can be enhanced by sulfidation.

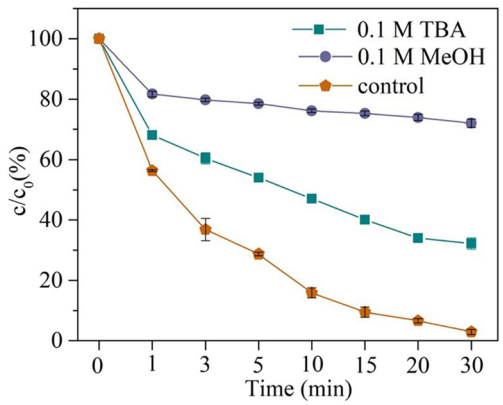

Fig. 10 Degradation of BPS in the S-nZVI/PS system with and without quenching agents MeOH and TBA. Conditions: $[PS]_0$ = 1.0 mM, $[BPS]_0$ = 20 μM, [S-nZVI] = 30 mg/L, pH = 5.6 ± 0.2, T = 25 °C

According to the above discussion, the reaction mechanism of BPS degradation by the S-nZVI/PS system could be proposed (Fig. 12). Firstly, Fe^0 is continuously converted to Fe^{2+} in several ways and diffused into solution (Eqs. (10-12)). Then, persulfate could be activated by Fe^{2+} to primarily

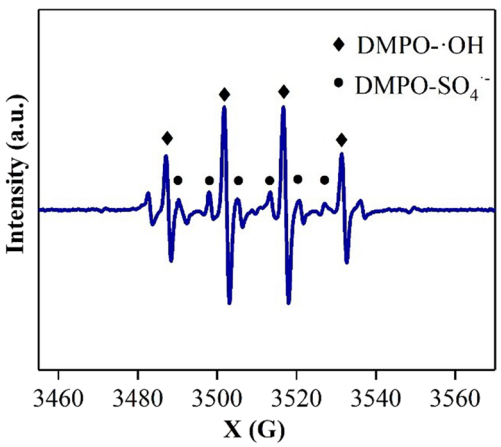

Fig. 11 EPR spectrum DMPO-OH and DMPO-SO_4 adduct in the S-nZVI/PS system at reaction times of 10 min. Conditions: $[PS]_0$ = 1.0 mM, $[BPS]_0$ = 20 μM, [S-nZVI] = 30 mg/L, pH = 5.6 ± 0.2, T = 25 °C

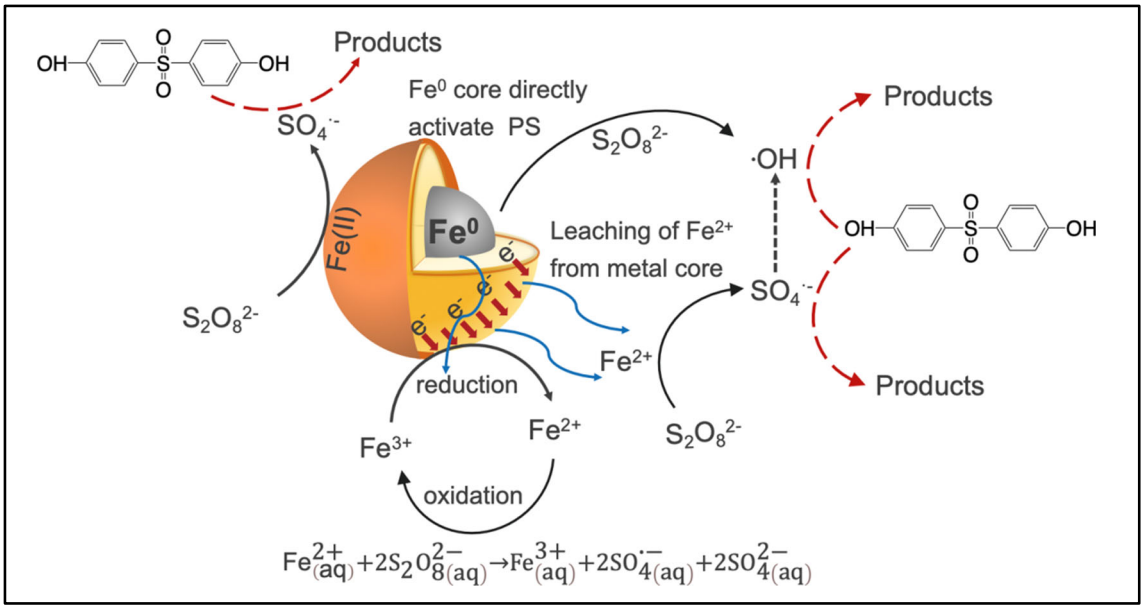

Fig. 12 Proposed mechanism of BPS degradation by S-nZVI/PS

generate powerful $SO_4^{\cdot-}$ with high redox potential, and Fe^{2+} oxidized into Fe^{3+} (Eq. 13). Meanwhile, ·OH can be generated through the reaction of $SO_4^{\cdot-}$ with H_2O or OH^- (Eq. (14)). Theoretically, Fe^{2+} can also be generated by the reaction of Fe^{3+} and Fe^0 core via Eq. (15). Secondly, at the same time, Fe^0 could also directly activate PS to produce ·OH to achieve the degradation of BPS (Eq. (16)). Finally, the degradation of BPS was carried out by the generated $SO_4^{\cdot-}$ and ·OH.

$$Fe^0_{(s)} + S_2O^{2-}_{8(aq)} \rightarrow Fe^{2+}_{(aq)} + 2SO^{2-}_{4(aq)} \quad (10)$$

$$Fe^0_{(s)} + \frac{1}{2}O_2 + H_2O \rightarrow Fe^{2+}_{(aq)} + 2OH^- \quad (11)$$

$$Fe^0_{(s)} + 2H_2O \rightarrow Fe^{2+}_{(aq)} + 2OH^- + H_2 \quad (12)$$

$$Fe^{2+}_{(aq)} + 2S_2O^{2-}_{8(aq)} \rightarrow Fe^{3+}_{(aq)} + 2SO^{\cdot-}_{4(aq)} + 2SO^{2-}_{4(aq)} \quad (13)$$

$$SO^{\cdot-}_4 + H_2O \rightarrow SO^{2-}_{4(aq)} + \cdot OH + H^+ \quad (14)$$

$$Fe^0 + 2Fe^{3+} \rightarrow 3Fe^{2+} \quad (15)$$

$$Fe^0_{(s)} + S_2O^{2-}_{8(aq)} + 2H_2O \rightarrow Fe^{2+} + 2\cdot OH + 2SO^{2-}_4 + 2H^+ \quad (16)$$

Furthermore, the presence of iron sulfides on the surface of nZVI played an important role in the degradation of BPS by S-nZVI/PS. On the one hand, it can promote the release of iron and the generation of $SO_4^{\cdot-}$ to accelerate the oxidation of BPS. On the other hand, before transferring into the solution, part of Fe (III) on the S-nZVI surface could be reduced to Fe (II) by S^{2-} (Eq. (17)). Then, the reactive species could be formed from the reaction of adsorbed persulfate with Fe (II) present in the S-nZVI surface (Eq. (18)).

$$2Fe\ (III) + HS^- \rightarrow 2Fe\ (II) + S^0 + H^+ \quad (17)$$

$$\equiv Fe\ (II) + S_2O^{2-}_{8(aq)} \rightarrow \equiv Fe\ (II)O_3SO_2SO_3^- \rightarrow \equiv Fe\ (III) + SO^{\cdot-}_{4(aq)} + SO^{2-}_{4(aq)} \quad (18)$$

where "≡Fe (II)" represents the Fe (II) on the S-nZVI surface.

The degradation of BPS could not only take place in homogeneous solution but also on the surface of S-nZVI, considering that about 27.5% of S-nZVI was removed by the S-nZVI alone, which was partly due to the adsorption of BPS on the surface of the S-nZVI. In conclusion, Fe^{2+}/PS, Fe^0/PS, and Fe (II)/PS reactions (in homogeneous solution and on the S-nZVI surface) and the adsorption of S-nZVI all contribute to BPS degradation in the S-nZVI/PS system.

Effects of PS concentration, S-nZVI dosage, and initial BPS concentration

The effects of initial concentration of PS on the BPS removal were experimentally investigated. The degradation rate of BPS increased with an increase in the concentration of PS (Fig. S4). In order to further explore the effects of initial concentration of PS on BPS removal rate, the kinetic behaviors were discussed. The BPS degradation data were fitted with the first-order kinetic equation. As depicted in Fig. S2, as the PS concentration increased from 0.5 to 10.0 mM, the reaction rate constant k_{obs} increased from 0.075 to 1.336 min^{-1} (Table 1). This may be explained that more free radicals were generated to degrade BPS with the increasing of PS concentration, resulting in higher removal efficiency of BPS.

Experiments of the effects of different dosages of S-nZVI on BPS removal were investigated; the results are illustrated in Fig. S5. When the S-nZVI dosages increased from 10, 20, 30, 40, and 50 mg/L, the BPS removal rates in 30 min reached 79.0%, 91.2%, 97.7%, 98.6%, and 100%, respectively. It was evident that the higher the S-nZVI concentration, the higher BPS removal rate was. In addition, as the S-nZVI dosage increased from 10 to 50 mg/L, the reaction rate constant k_{obs} was increased from 0.045 to 0.249 min^{-1}. And the k_{obs} for BPS removal at 50 mg/L is almost 5.5 times higher than that of 10 mg/L. With an increase in S-nZVI dosage, the available active sites of S-nZVI were correspondingly increased and more iron leaching that could induce PS to generate more free radicals, thereby accelerating the BPS degradation.

The results of the effects of initial BPS concentration on BPS removal by S-nZVI/PS are shown in Fig. S6. As expected, the removal efficiency of BPS decreased with an increase in the concentration of BPS. When the initial concentration of BPS increased from 10 to 40 μM, the removal efficiency of BPS decreased from 100 to 84.8%. While the effect of initial BPS concentration is hard to be analyzed from the temporal evolution of normalized concentration, the initial rate was estimated as a better tool to study this variable. Thus, as observed in Fig. S6, an increase of initial BPS concentration enhanced the degradation rate of the contaminant (Solis et al. 2020).

Effects of pH and temperature

To investigate the effects of initial pH on BPS degradation by S-nZVI/PS, batch experiments were performed at different pH values (Fig. S7). BPS degradation rates decreased according to the following order: pH 5.60 > 7.01 > 3.13 > 9.35 > 11.21. It is noteworthy that the efficient degradation of BPS (87.2–97.7%) could be achieved over a broad pH range of 3.13–9.35, and the degradation rate was greatly retarded (10%) at a pH value of 11.21.

Interestingly, previous studies reported that acidic pH favored degradation of organic pollutants in the nZVI-activated PS process. In our study, faster degradation of BPS was found at pH 5.60 than at pH 3.13. This may be attributed to the higher production of Fe^{2+} under acidic conditions, which may lead to scavenging of $SO_4^{\cdot-}$ (Eq. (5)), resulting in lower k_{obs} for initial pH of 3.13. A gradual drop of BPS degradation with the increasing of pH was observed, which could be attributed to the iron oxides/hydroxides formed on the surface of S-nZVI, and then impede the reaction between S-nZVI and PS. When the strong alkaline condition was adopted (pH = 11.21), Fe^{2+} may react with the hydroxyl ion or sulfate ion to form corresponding precipitated hydroxide and ferrous sulfate. And the lower solubility of Fe^{2+} would decrease its ability to activate PS. The similar phenomenon was observed in reports by Rayaroth et al., who concluded the decrease in catalytic activity of Fe^0 at alkaline pH was to be expected due to its inactivation by the precipitated oxides, hydroxides, and sulfates (Rayaroth et al. 2017). Overall, S-nZVI can efficiently activate BPS across a wide range of pH (3.13–9.35).

Batch experiments were carried out at different temperatures of 15, 25, and 35 °C to investigate the effects of temperature on the degradation of BPS by S-nZVI/PS. As shown in Fig. S8, the degradation efficiency increased with an increase in temperature from 15 to 35 °C. The results demonstrate that higher temperature has a positive effect on generating free radicals ($SO_4^{\cdot-}$ and ·OH) to degrade BPS.

The reusability of S-nZVI

As we all know, the reusability of a catalyst plays an important role in the applicability of iron-based particles. In order to evaluate the reusability of S-nZVI for removing BPS from the solution, the S-nZVI particles were repeatedly used 4 times, and the leached total iron ion concentration was measured after reaction. As seen in Fig. S9, the removal efficiency of BPS by the S-nZVI/PS system gradually decreased from 97.7%, to 88.9%, 61.2%, and 50.8% as the particles were used in the first, second, third, and fourth cycle, respectively. The decline of BPS removal efficiency in S-nZVI/PS system was possibly attributed to the following factors: (1) the corrosion of the S-nZVI particles could result in a decrease of Fe^0 core content, and the leached total iron ion concentration was decreased gradually to 7.65, 4.56, and 3.45 mg/L, after the second, third, and fourth cycle experiments (seen in Fig. S8(b)); (2) degradation intermediates adsorbed and corrosion products on the surface of the S-nZVI could block the active sites and inhibit the transfer of electron, which would weaken the PS activation and BPS degradation.

Conclusions

In this study, a series of S-nZVI composites were synthesized and employed in activating PS to remove BPS from water. S-nZVI was found to be more efficient than nZVI in activating PS to degrade BPS, especially at high BPS concentration. The aggregation and passivation of nZVI could be improved by adding an iron sulfide layer, which could also enhance the electron transfer at appropriate molar ratio of S/Fe. The property of nZVI for PS activation can be enhanced by sulfidation. Higher PS concentration and S-nZVI dosage will enhance BPS degradation by S-nZVI/PS. BPS was efficiently degraded in solutions with a wide range of

initial pH (3.13–9.35). $SO_4^{\cdot-}$ and ·OH were the predominant oxidants with respect to BPS degradation. Fe^{2+}/PS, Fe^0/PS, and Fe (II)/PS reactions (in homogeneous solution and on the surface of S-nZVI) and the adsorption of S-nZVI all contribute to BPS degradation in the S-nZVI/PS system. Overall, these results along with the low energy and low chemical requirements suggest that the PS activated with the S-nZVI system has a strong potential for the application in water treatment and environmental remediation.

Supplementary Information The online version contains supplementary material available at https://doi.org/10.1007/s11356-021-16156-8.

Availability of data and materials Not applicable

Author's contribution JC performed the relevant experiments of this research and was a major contributor in writing the manuscript. YZ edited the manuscript and provided financial support. The authors read and approved the final manuscript.

Funding This research was supported by the National Science and Technology Major Project of China - Water Pollution Control and Treatment (2017ZX07201004).

Declarations

Ethics approval and consent to participate Not applicable.

Consent for publication Not applicable.

Competing interests The authors declare no competing interests.

References

Ahsan N, Ullah H, Ullah W, Jahan S (2018) Comparative effects of bisphenol S and bisphenol A on the development of female reproductive system in rats; a neonatal exposure study. Chemosphere 197:336–343

Azevedo LF, Hornos Carneiro MF, Dechandt CRP, Cassoli JS, Alberici LC, Barbosa F Jr (2020) Global liver proteomic analysis of Wistar rats chronically exposed to low-levels of bisphenol A and S. Environmental Research 182:109080

Cai J, Zhang Y (2020) Enhanced reduction of bromate from water by AC/S-nZVI: performance and mechanism. Journal of Environmental Engineering 146(9):04020107

Cao Z, Liu X, Xu J, Zhang J, Yang Y, Zhou J, Xu X, Lowry GV (2017) Removal of antibiotic florfenicol by sulfide-modified nanoscale zero-valent iron. Environ Sci Technol 51(19):11269–11277

Champmartin C, Marquet F, Chedik L, Decret MJ, Aubertin M, Ferrari E, Grandclaude MC, Cosnier F (2020) Human in vitro percutaneous absorption of bisphenol S and bisphenol A: a comparative study. Chemosphere 252:126525

Danzl E, Sei K, Soda S, Ike M, Fujita M (2009) Biodegradation of bisphenol A, bisphenol F and bisphenol S in seawater. Int J Environ Res Public Health 6(4):1472–1484

Dong H, Hou K, Qiao W, Cheng Y, Zhang L, Wang B, Li L, Wang Y, Ning Q, Zeng G (2019) Insights into enhanced removal of TCE utilizing sulfide-modified nanoscale zero-valent iron activated persulfate. Chemical Engineering Journal 359:1046–1055

Dong H, Ning Q, Li L, Wang Y, Wang B, Zhang L, Tian R, Li R, Chen J and Xie Q (2020) A comparative study on the activation of persulfate by bare and surface-stabilized nanoscale zero-valent iron for the removal of sulfamethazine. Separation and Purification Technology 230

Dong H, Zhang C, Deng J, Jiang Z, Zhang L, Cheng Y, Hou K, Tang L, Zeng G (2018) Factors influencing degradation of trichloroethylene by sulfide-modified nanoscale zero-valent iron in aqueous solution. Water Research 135:1–10

Du J, Bao J, Lu C, Werner D (2016) Reductive sequestration of chromate by hierarchical FeS@Fe(0) particles. Water Research 102:73–81

Freitas JM, Wachter N and Rocha-Filho RC (2020) Determination of bisphenol S, simultaneously to bisphenol A in different water matrices or solely in electrolyzed solutions, using a cathodically pretreated boron-doped diamond electrode. Talanta 217

Fu C, Yi X, Liu Y, Zhou H (2020) Cu^{2+} activated persulfate for sulfamethazine degradation. Chemosphere 257:127294

Fu R, Yang Y, Xu Z, Zhang X, Guo X, Bi D (2015) The removal of chromium (VI) and lead (II) from groundwater using sepiolite-supported nanoscale zero-valent iron (S-NZVI). Chemosphere 138:726–734

Gayathri P, Praveena Juliya Dorathi R, Palanivelu K (2010) Sonochemical degradation of textile dyes in aqueous solution using sulphate radicals activated by immobilized cobalt ions. Ultrasonics Sonochemistry 17(3):566–571

Han Y, Yan W (2016) Reductive dechlorination of trichloroethene by zero-valent iron nanoparticles: reactivity enhancement through sulfidation treatment. Environ Sci Technol 50(23):12992–13001

Hussain I, Li M, Zhang Y, Li Y, Huang S, Du X, Liu G, Hayat W, Anwar N (2017) Insights into the mechanism of persulfate activation with nZVI/BC nanocomposite for the degradation of nonylphenol. Chemical Engineering Journal 311:163–172

Jia T, Zhang B, Huang L, Wang S, Xu C (2019) Enhanced sequestration of Cr(VI) by copper doped sulfidated zerovalent iron (SZVI-Cu): characterization, performance, and mechanisms. Chemical Engineering Journal 366:200–207

Jiang Z, Li J, Jiang D, Gao Y, Chen Y, Wang W, Cao B, Tao Y, Wang L, Zhang Y (2020) Removal of atrazine by biochar-supported zero-valent iron catalyzed persulfate oxidation: reactivity, radical production and transformation pathway. Environmental Research 184:109260

Kim C, Ahn JY, Kim TY, Hwang I (2020) Mechanisms of electro-assisted persulfate/nano-Fe(0) oxidation process: roles of redox mediation by dissolved Fe. Journal of Hazardous materials 388:121739

Kim C, Ahn JY, Kim TY, Shin WS, Hwang I (2018) Activation of persulfate by nanosized zero-valent iron (NZVI): mechanisms and transformation products of NZVI. Environmental Science and Technology 52(6):3625–3633

Kim EJ, Kim JH, Azad AM, Chang YS (2011) Facile synthesis and characterization of Fe/FeS nanoparticles for environmental applications. ACS Appl Mater Interfaces 3(5):1457–1462

Kim EJ, Kim JH, Chang YS, Turcio-Ortega D, Tratnyek PG (2014) Effects of metal ions on the reactivity and corrosion electrochemistry of Fe/FeS nanoparticles. Environ Sci Technol 48(7):4002–4011

Li Y, Zhao X, Yan Y, Yan J, Pan Y, Zhang Y and Lai B (2019) Enhanced sulfamethoxazole degradation by peroxymonosulfate activation with sulfide-modified microscale zero-valent iron ($S\text{-}mFe^0$): performance, mechanisms, and the role of sulfur species. Chemical Engineering Journal 376.

Liang C, Huang CF, Mohanty N, Kurakalva RM (2008) A rapid spectrophotometric determination of persulfate anion in ISCO. Chemosphere 73(9):1540–1543

Liu Y, Guo H, Zhang Y, Cheng X, Zhou P, Wang J and Li W (2019) Fe@C carbonized resin for peroxymonosulfate activation and bisphenol S degradation. Environmental Pollution 252(Pt B), 1042-1050

Lu X, Zhao J, Wang Q, Wang D, Xu H, Ma J, Qiu W, Hu T (2019) Sonolytic degradation of bisphenol S: effect of dissolved oxygen and peroxydisulfate, oxidation products and acute toxicity. Water Research 165:114969

Mercado DF, Bracco LLB, Arques A, Gonzalez MC, Caregnato P (2018a) Reaction kinetics and mechanisms of organosilicon fungicide flusilazole with sulfate and hydroxyl radicals. Chemosphere 190:327–336

Mercado DF, Cipollone M, González MC, Sánchez FH (2018b) Yerba mate applications: magnetic response of powders and colloids of iron oxide nanoparticles coated with Ilex paraguariensis derivatives. Journal of Magnetism and Magnetic Materials 462:13–21

Mercado DF and Weiss R (2018) Polydimethylsiloxane as a matrix for the stabilization and immobilization of zero-valent iron nanoparticles. Applications to dehalogenation of environmentally deleterious molecules. Journal of the Brazilian Chemical Society

Ning H, Zhai Y, Li S, Liu X, Wang T, Wang B, Liu Y, Qiu Z, Li C, Zhu Y (2020) Fe(II) activated persulfate assisted hydrothermal conversion of sewage sludge: focusing on nitrogen transformation mechanism and removal effectiveness. Chemosphere 244:125473

Rajajayavel SR, Ghoshal S (2015) Enhanced reductive dechlorination of trichloroethylene by sulfidated nanoscale zerovalent iron. Water Research 78:144–153

Rayaroth MP, Lee C-S, Aravind UK, Aravindakumar CT, Chang Y-S (2017) Oxidative degradation of benzoic acid using Fe^{0} and sulfidized Fe^{0}-activated persulfate: a comparative study. Chemical Engineering Journal 315:426–436

Roy K, Agarkoti C, Malani RS, Thokchom B, Moholkar VS (2020) Mechanistic study of sulfadiazine degradation by ultrasound-assisted Fenton-persulfate system using yolk-shell Fe_3O_4@hollow@$mSiO_2$ nanoparticles. Chemical Engineering Science 217

Solis RR, Mena IF, Nadagouda MN, Dionysiou DD (2020) Adsorptive interaction of peroxymonosulfate with graphene and catalytic assessment via non-radical pathway for the removal of aqueous pharmaceuticals. Journal of Hazardous materials 384:121340

Song S, Su Y, Adeleye AS, Zhang Y, Zhou X (2017) Optimal design and characterization of sulfide-modified nanoscale zerovalent iron for diclofenac removal. Applied Catalysis B: Environmental 201:211–220

Su Y, Adeleye AS, Huang Y, Zhou X, Keller AA, Zhang Y (2016) Direct synthesis of novel and reactive sulfide-modified nano iron through nanoparticle seeding for improved cadmium-contaminated water treatment. Sci Rep 6:24358

Su Y, Adeleye AS, Keller AA, Huang Y, Dai C, Zhou X, Zhang Y (2015) Magnetic sulfide-modified nanoscale zerovalent iron (S-nZVI) for dissolved metal ion removal. Water Research 74:47–57

Sun Y, Gu M, Lyu S, Brusseau ML, Li M, Lyu Y, Xue Y, Qiu Z, Sui Q (2020) Efficient removal of trichloroethene in oxidative environment by anchoring nano FeS on reduced graphene oxide supported nZVI catalyst: the role of FeS on oxidant decomposition and iron leakage. Journal of Hazardous materials 392:122328

Wang B, Li YN, Wang L (2019) Metal-free activation of persulfates by corn stalk biochar for the degradation of antibiotic norfloxacin: activation factors and degradation mechanism. Chemosphere 237: 124454

Wang Q, Lu X, Cao Y, Ma J, Jiang J, Bai X, Hu T (2017) Degradation of bisphenol S by heat activated persulfate: kinetics study, transformation pathways and influences of co-existing chemicals. Chemical Engineering Journal 328:236–245

Wu J, Wang B, Cagnetta G, Huang J, Wang Y, Deng S and Yu G (2020) Nanoscale zero valent iron-activated persulfate coupled with Fenton oxidation process for typical pharmaceuticals and personal care products degradation. Separation and Purification Technology 239

Wu X, Gu X, Lu S, Xu M, Zang X, Miao Z, Qiu Z, Sui Q (2014) Degradation of trichloroethylene in aqueous solution by persulfate activated with citric acid chelated ferrous ion. Chemical Engineering Journal 255:585–592

Xu Z, Gao Y, Sun Z, Zhang D, Zhou Y and Chen W (2020) New insights into the reinforced reduction performance of Fe^{0}/C internal electrolysis activated by persulfate for p-nitrophenol removal. Chemosphere 254.

Yan J, Han L, Gao W, Xue S, Chen M (2015) Biochar supported nanoscale zerovalent iron composite used as persulfate activator for removing trichloroethylene. Bioresource Technology 175:269–274

Yang X, Zhang S, Liu L, Ju M (2020) Study on the long-term effects of DOM on the adsorption of BPS by biochar. Chemosphere 242: 125165

Zhang T, Zhou T, He L, Xu D and Bai L (2020) Oxidative degradation of rhodamine B by Ag@CuO nanocomposite activated persulfate. Synthetic Metals 267